Available online at www.sciencedirect.com

SCIENCE DIRECT

Biochimica et Biophysica Acta 1675 (2004) 12–20

BIOCHIMICA ET BIOPHYSICA ACTA

BBA

http://www.elsevier.com/locate/bba

Further development of Axisymmetric Drop Shape Analysis-Captive Bubble for pulmonary surfactant related studies

Y.Y. Zuo[a], M. Ding[b], D. Li[a], A.W. Neumann[a,*]

[a]Department of Mechanical and Industrial Engineering, University of Toronto, 5 King's College Road, Toronto, ON, Canada, M5S 3G8
[b]Division of Engineering Science, Faculty of Applied Science and Engineering, University of Toronto, 40 St. George Street, Toronto, ON, Canada, M5S 2E4

Received 12 April 2004; received in revised form 23 July 2004; accepted 3 August 2004
Available online 21 August 2004

Abstract

The methodology combining Axisymmetric Drop Shape Analysis (ADSA) with a captive bubble (ADSA-CB) facilitates pulmonary surfactant related studies. The accuracy of ADSA-CB is crucially dependent on the quality of the bubble profile extracted from the raw image. In a previous paper, an image analysis scheme featuring a Canny edge detector and a Axisymmetric Liquid Fluid Interfaces-Smoothing (ALFI-S) algorithm was developed to process captive bubble images under a variety of conditions, including images with extensive noise and/or lack of contrast. A new version of ADSA-CB based on that image analysis scheme is developed and applied to pulmonary surfactant and pulmonary surfactant–polymer systems. The new version is found to be highly noise-resistant and well self-adjusting.

Keywords: Axisymmetric Drop Shape Analysis (ADSA); Captive Bubble (CB); Pulmonary surfactant; Image analysis; Dynamic surface tension measurement

1. Introduction

To study the surface activity of pulmonary surfactant, a captive bubble surfactometer (CBS) was first introduced by Schürch et al. [1,2]. In CBS, the ceiling of the captive bubble chamber is coated with agar gel, which ensures that the area of contact between bubble and chamber is completely hydrophilic. Consequently, an air bubble is separated from the ceiling by a very thin wetting film of the surrounding aqueous liquid, thus avoiding adhesion to the solid and eliminating the potential pathways for film leakage. Without film leakage, a stable surface tension less than 2 mJ/m^2, mimicking the physiological surface tension in lungs, can be readily obtained by using a moderate compression ratio [3]. The bubble images taken in the experiments were enhanced by an image processing program and the bubble profiles were extracted by a simple thresholding method [4]. The remaining outliers were removed by manual editing. The bubble height (h) and diameter (d) were then determined manually from the bubble profile. Surface tension, bubble area and volume were calculated by substituting the ratio of bubble height to diameter (h/d) into three corresponding polynomial fitting equations, respectively. The surface tension polynomial was modified from the formulas derived by Malcolm and Elliott [5]. The polynomials of area and volume were regressed from the measurements of a series of sample bubbles with a wide range of h/d.

For a more sophisticated evaluation, Axisymmetric Drop Shape Analysis (ADSA) can be used to analyze the segmented bubble profile. ADSA is a surface tension measurement methodology first introduced by Rotenberg et al. [6] and has been significantly improved by del Río and Neumann [7]. In ADSA, surface tension of the bubble (or drop) profile is identified by the best fitted theoretical profile given by the classical Laplace equation of capillarity. Details of the related mathematics can be found elsewhere [6–8].

* Corresponding author. Tel.: +1 416 978 1270; fax: +1 416 978 7753.
E-mail address: neumann@mie.utoronto.ca (A.W. Neumann).

0304-4165/$ - see front matter
doi:10.1016/j.bbagen.2004.08.003

The combination of the captive bubble method and ADSA facilitates accurate measurement of surface tension, bubble area and volume in a lung surfactant system [9]. The first version of ADSA-Captive Bubble (CB) methodology was developed by Prokop et al. [10]. In that version, a global thresholding method was used to segment the bubble profile; then, a Fifth Order Polynomial Fitting (FOPF) strategy was used to smooth the extracted edge. That version of ADSA-CB has been used to analyze the formation, compressibility and stability of lung surfactant films [10,11]. However, it suffers from a serious problem: it is not robust in the presence of noise. When noisy images are processed, the ADSA results tend to lack accuracy and consistency. This limitation is due to poor noise resistance of the edge detection and smoothing scheme [12]. To solve this problem, a new image analysis strategy was recently developed [12]. This new scheme uses a Canny edge detector [13] to replace thresholding and a novel edge smoothing technique, termed Axisymmetric Liquid Fluid Interfaces-Smoothing (ALFI-S), to replace FOPF. It is found that this method succeeds in processing captive bubble images under a variety of conditions, including images with considerable noise and/or lack of contrast.

In the present paper, a new version of the ADSA-CB software is developed. It is based on an advanced image analysis scheme [12]. This new version of ADSA-CB is demonstrated by studying the aging processes of pulmonary surfactant and pulmonary surfactant–polymer systems. Two categories of aging processes are studied. One is a static experiment, in which the evolution of a stationary bubble is continuously monitored. The other is a dynamic cycling experiment, in which the bubble area is periodically increased and decreased, by pumping surfactant liquid in and out of the bubble chamber, by means of a motorized syringe. In both cases, film formation is due to adsorption from bulk lung surfactant suspensions. In such systems, due to turbidity of the test liquids, captive bubble images suffer from extensive optical noise. However, the methodology developed in this paper is also applicable to spreading films.

2. Materials and methods

2.1. Materials

Bovine lipid extract surfactant (BLES Biochemicals, London, ON, Canada) was prepared from bovine natural lung surfactant obtained by bronchopulmonary lavage with organic extraction. BLES contains about 98% phospholipids and 2% proteins. The main tensioactive component is dipalmitoylphosphatidylcholine (DPPC), which accounts for 44% of the phospholipid components. The protein components in BLES are only surfactant-associated proteins B (SP-B) and C (SP-C). High molecular weight hydrophilic proteins, SP-A and SP-D, were removed from the extracts. BLES was stored frozen in sterilized vials with an initial concentration of 27 mg phospholipids/ml. It was diluted to the desired concentration by a salt solution of 0.6% NaCl+1.5 mM $CaCl_2$ on the day of the experiment. Polyethylene glycol (PEG) (M.W. 10,000, Sigma, St. Louis, MO, USA) was used without further purification. Dry PEG was added to the above diluted BLES in the desired concentration. The water used in the experiments was demineralized and doubly distilled.

2.2. Experimental protocol

The experimental setup is the same as described before [12]. The captive bubble chamber used in the current study is made of stainless steel without further treatment of the ceiling. This removes the possibility that material from the wetting film separating the bubble from the ceiling may diffuse into a coating layer.

In the static experiments, a mixture of 0.5 mg/ml BLES and 50 mg/ml PEG was studied as it yields an extremely noisy background. A pure oxygen bubble was used in the current work. Due to the difference between the partial pressure of O_2 in the gas phase and the liquid phase (~21%), a measurable bubble shrinkage is achieved in a rather short experimental period (10 min). In the dynamic cycling experiments, the film formation was done by rapid adsorption from a 0.5 mg/ml BLES suspension (film formation completed within 5 s). The adsorbed lung surfactant film was subsequently compressed and expanded by a motor-driven syringe at a period of 5 s per cycle, which approximately mimics the typical respiratory frequency of an healthy adult (12 breaths per minute) [14]. All experiments were conducted at 37 °C.

2.3. Image analysis strategy

The study of a pulmonary surfactant system necessitates an image analysis scheme robust against noise. This is important due to two facts: (1) Pulmonary surfactants are a dispersion of more or less insoluble phospholipid aggregates or vesicles. At a phospholipid concentration as high as 1–2 mg/ml, the sample becomes murky and the bubble edge is invisible. (2) When pulmonary surfactants are mixed with SP-A or some nonionic polymer, e.g., PEG, fairly large aggregates are created by a polymer-induced depletion force [15,16]. These large aggregates can significantly improve the adsorption of the phospholipids onto the air–liquid interface and therefore efficiently decrease surface tension [17]. However, the presence of these aggregates causes considerable optical noise in the image, thus compromising the applicability of a captive bubble method in such studies. The main difficulty is due to the fact that the image analysis methods commonly used so far, such as thresholding [4,10] and SOBEL edge detector [18], fail to detect an undisturbed edge from a noisy image.

A general image analysis scheme consists of edge detection, edge smoothing, and, if necessary, edge correc-

Table 1
ADSA results[a] in conjunction with thresholding as a function of threshold value (T)

T	Surface tension (mJ/m^2)	Area (cm^2)	Volume (cm^3)	Curvature at apex (cm^{-1})
20	23.08	0.3552	0.01854	4.306
40	23.30	0.3567	0.01862	4.303
60	23.28	0.3579	0.01872	4.289
80	23.58	0.3595	0.01891	4.291
100	23.64	0.3603	0.01899	4.285
120	23.80	0.3621	0.01919	4.273
140	23.74	0.3627	0.01927	4.263
160	Failed			
Mean[b]	$23.49 \pm 6.4 \times 10^{-3}$	$0.3592 \pm 6.6 \times 10^{-5}$	$0.01889 \pm 6.6 \times 10^{-6}$	$4.287 \pm 3.6 \times 10^{-4}$

[a] The calculations are based on a captive bubble image in the mixture of 0.5 mg/ml BLES and 50 mg/ml PEG (10,000) using the whole profile without correction of optical distortion.

[b] The mean values for ADSA results are shown with 95% confidence intervals to illustrate the extent of the trend in the results for the different quantities.

tion. The image analysis scheme used here was recently developed and described [12]. This new scheme features a combination of a Canny edge detector in the edge detection and a smoothing algorithm called ALFI-S. The Canny edge detector is highly noise-resistant and thus very suitable for processing captive bubble images. Edge smoothing was also found to be necessary. In the new method [12], edge smoothing is performed in two steps. First, any assumed edge point far away from the main bubble profile (isolated noise) is eliminated by measuring coherence of adjacent points. Then, those noise points attached to the main edge profile, termed adhering noise, are removed by ALFI-S. ALFI-S is a tool to smooth an obscured or disturbed Laplacian profile. In ALFI-S, an experimental profile is fitted to the best matched Laplacian curve and questionable edge points away from the theoretical curve by 3σ are rejected as outliers.(σ is the standard deviation evaluated from the distance between each experimental edge point and the closest theoretical point.) ALFI-S is performed iteratively until no more outliers are found. Detailed implementation of this image analysis scheme can be found elsewhere [12].

If sophisticated measurement is required, edge correction needs to be conducted subsequently. Edge correction refers to the correction of optical distortion generated by the image acquisition hardware (microscope, camera and digital video processor). The distortion correction scheme used in the current program was first implemented by Cheng [19] and modularized by Hoorfar and Neumann [20].

3. Results

3.1. Parameter dependence of thresholding and Canny edge detector

To achieve optimal performance, any edge detector requires user-specified parameters a priori. Thresholding

Table 2
ADSA results[a] in conjunction with the Canny edge detector as a function of standard deviation (σ_G) of the Gaussian filter

σ_G	Surface tension (mJ/m^2)	Area (cm^2)	Volume (cm^3)	Curvature at apex (cm^{-1})	Remaining edge points[c]	Deleted edge points[c]	ALFI-S iteration[c]
0.8	Failed						
1.0	23.65	0.3612	0.01906	4.271	695	171	9
1.2	23.68	0.3613	0.01906	4.272	701	153	8
1.4	23.74	0.3616	0.01908	4.274	748	132	8
1.6	23.74	0.3616	0.01908	4.274	743	124	7
1.8	23.74	0.3616	0.01908	4.274	747	76	7
2.0	23.72	0.3615	0.01908	4.273	752	81	7
2.2	23.70	0.3615	0.01907	4.272	762	23	5
2.4	23.70	0.3615	0.01907	4.272	763	24	5
2.6	23.70	0.3615	0.01907	4.272	759	15	4
2.8	23.64	0.3614	0.01906	4.270	741	16	4
3.0	23.63	0.3615	0.01906	4.269	669	14	4
3.2	23.64	0.3615	0.01906	4.269	667	16	4
3.4	23.63	0.3615	0.01906	4.269	666	17	5
3.6	23.64	0.3614	0.01906	4.270	727	16	4
3.8	23.64	0.3614	0.01906	4.270	724	16	4
4.0	23.64	0.3614	0.01906	4.270	724	16	4
Mean[b]	$23.677 \pm 6.69 \times 10^{-4}$	$0.36146 \pm 1.71 \times 10^{-6}$	$0.019067 \pm 1.37 \times 10^{-7}$	$4.2713 \pm 2.85 \times 10^{-5}$	724	57	5.6

[a] The calculations are based on the captive bubble image coincident in Table 1 using the whole profile without correction of optical distortion.

[b] The mean values for ADSA results are shown with 95% confidence intervals to illustrate the extent of the trend in the results for the different quantities.

[c] The last three columns list the numbers of remaining and deleted edge points after ALFI-S, and the number of iterations of ALFI-S.

requires an intensity value which serves as a threshold (T) to separate the foreground from the background. In the Canny edge detector, the standard deviation (σ_G) of the Gaussian filter plays an operative role. To compare the dependence of ADSA results on the user-specified parameters of thresholding and the Canny edge detector, a captive bubble image in a mixture of 0.5 mg/ml BLES and 50 mg/ml PEG is analyzed by varying T and σ_G, respectively. For the purpose of comparison, calculation is carried out using the whole profile without correction of optical distortion.

Table 1 shows the ADSA results of thresholding. When the threshold value is as high as 160, ADSA results deviate unreasonably, indicating failure of ADSA. It is noticed that there is a clear trend in the ADSA results, especially for the bubble area and volume. That is, both the bubble area and volume increase about 2% and 4%, respectively, with increasing threshold value. Furthermore, there are no criteria to give preference to any one threshold value over a wide range.

The dependence of the Canny edge detector on σ_G is examined in Table 2. It is clear that over a large range of σ_G, from 1.0 to 4.0, the ADSA results are very consistent and there is no apparent trend. The 95% confidence intervals associated with the mean values using the Canny edge detector are generally one order of magnitude less than those using thresholding. The Canny edge detector is far less sensitive to the user-specified parameter than thresholding.

Actually, the stable performance shown in Table 2 has to be attributed to the combined effect of the Canny edge detector and ALFI-S. To elucidate this point, the remaining and deleted edge points after ALFI-S is applied are also listed in Table 2. It is noted that for different values of σ_G, the numbers of finally remaining edge points are similar and around 720. However, a considerably larger number of points are removed by ALFI-S when σ_G is small. Accordingly, more iterations are needed. This result is due to the fact that if σ_G is small, the Gaussian filter used in the Canny

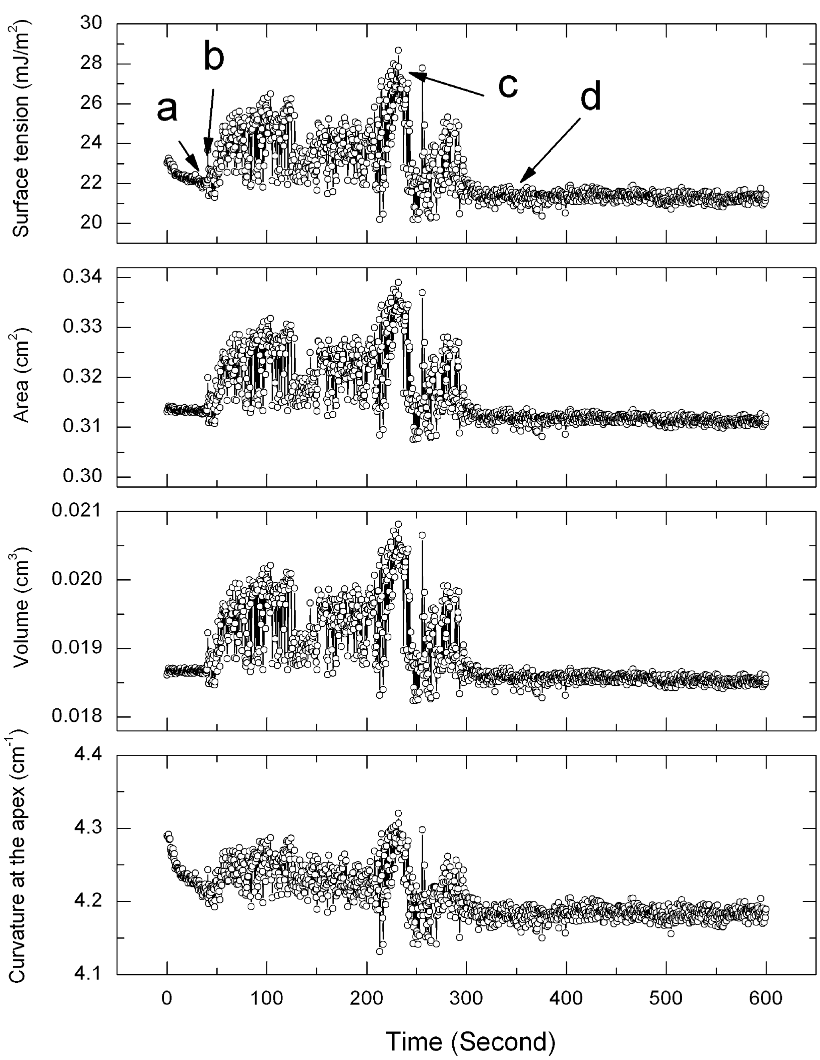

Fig. 1. ADSA results for a static experiment (oxygen bubble in the mixture of 0.5 mg/ml BLES and 50 mg/ml PEG) analyzed using the previous version of ADSA-CB. The “a”, “b”, “c” and “d” denote the time points 40.07, 40.48, 226.95 and 350.54 s, respectively.

edge detector is not sufficient to suppress all of the noise. Under these circumstances, the edge smoothing procedure, ALFI-S, is responsible for further noise reduction, which renders the final number of edge points relatively constant. When σ_G is decreased to 0.8, more noise remains after the edge detection than can be removed by ALFI-S, thereby causing the failure of ADSA.

3.2. Application of the new version of ADSA-CB to lung surfactant related studies

The new version of ADSA-CB was demonstrated by studying the surface aging process of lung surfactant systems in which the physicochemical properties of the system vary with respect to time. Both a static bubble and an oscillating bubble were studied as examples of different aging processes. The experiments were analyzed using both the new and the previous version of ADSA-CB.

3.2.1. Static experiments

Fig. 1 shows a typical ADSA output calculated by the previous version of ADSA-CB. Here, in a 10-min period, an oxygen bubble is held undisturbed in the surrounding quiescent aqueous mixture of 0.5 mg/ml BLES and 50 mg/ml PEG. Due to the considerable scatter, no significant trend can be observed in Fig. 1. The extreme jumps, especially between 40 and 300 s, in surface tension, bubble area, volume and curvature at the apex are not physically likely. A close scrutiny of these unsatisfactory results requires examination of the raw images in question. Fig. 2

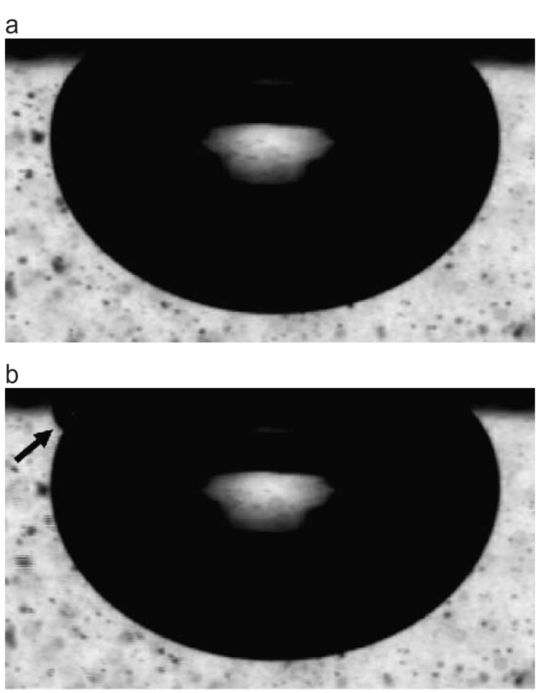

Fig. 2. Two captive bubble images at time (a) 40.07 and (b) 40.48 s. A satellite bubble (indicated by an arrow) is formed between acquisition of the two images. The denotations of these two images correspond to “a” and “b” in Figs. 1 and 3.

shows the two images corresponding to the time points denoted by “a” and “b”, respectively, in Fig. 1. As shown in Fig. 2(b), at time 40.48 s, a small bubble (as indicated by the arrow in Fig. 2(b)) suddenly appears at the three-phase contact region. The sudden formation of small bubbles in a captive bubble chamber was also reported by others and called “satellite bubble formation” [21]. The satellite bubbles usually appear at a low system pressure or during bubble injection. Previous efforts to remove the satellite bubbles include degassing the liquid and performing rapid bubble injection [21]. In terms of image analysis, these satellite bubbles are “adhering noise” in an otherwise acceptable image (see Fig. 2(a) at 40.07 s). Thanks to the fast acquisition speed of ADSA, it is possible to visualize this change. Adhering noise around the three-phase contact line has the most deleterious effect on the surface tension measurement [22]. Due to this adhering noise, a jump in the surface tension value from 22.17 to 23.67 mJ/m^2 occurs within 0.4 s. At 226.95 s (denoted by “c” in Fig. 1), the surface tension value reaches a local maximum of 27.99 mJ/m^2 due to slightly swelling of the satellite bubble; at 350.54 s (denoted by “d” in Fig. 1), the measurement goes back to a physically reasonable value of 21.10 mJ/m^2 due to shrinkage of the satellite bubble.

The same set of images was also processed using the new version of ADSA-CB. As shown in Fig. 3, the new results are more consistent than those shown in Fig. 1. At the onset of recording data, the surface tension is already less than 24 mJ/m^2, indicating that essentially complete adsorption has occurred. As time goes on, the surface tension gradually decreases to a value below 21.5 mJ/m^2. This decrease in surface tension is due to film compression or “shrinkage” indicated by the decrease of bubble area (see Fig. 3). The noticeable shrinkage is possibly due to oxygen diffusion out of the bubble since a difference in oxygen partial pressure exists between the gas side (~100%) and liquid side (~21%). The volume decrease (see Fig. 3) also suggests a decrease of the mass of gas in the bubble. The surface tension values corresponding to the four points denoted by “a”, “b”, “c” and “d” in Fig. 3 (the denotations are identical to those in Fig. 1) are 22.20, 22.14, 21.55, and 21.44 mJ/m^2, respectively. It is noted that at 226.95 s, there is a considerable difference (6 mJ/m^2) in the surface tension values between the two types of analysis. The result obtained from the new version is obviously more reliable.

It is also noted that local fluctuations in the ADSA results, especially in bubble area and volume, still exist. However, this is not an artefact of ADSA but a manifestation of physical reality. That is, adsorption of surfactant molecules onto the air–liquid interface is a random process. Since the shape of a captive bubble is controlled by the surface tension, fluctuation in bubble area due to transient adsorption or desorption of surfactant molecules is inevitable. The bubble volume in the current study is also affected, albeit to a lesser extent than bubble area, by

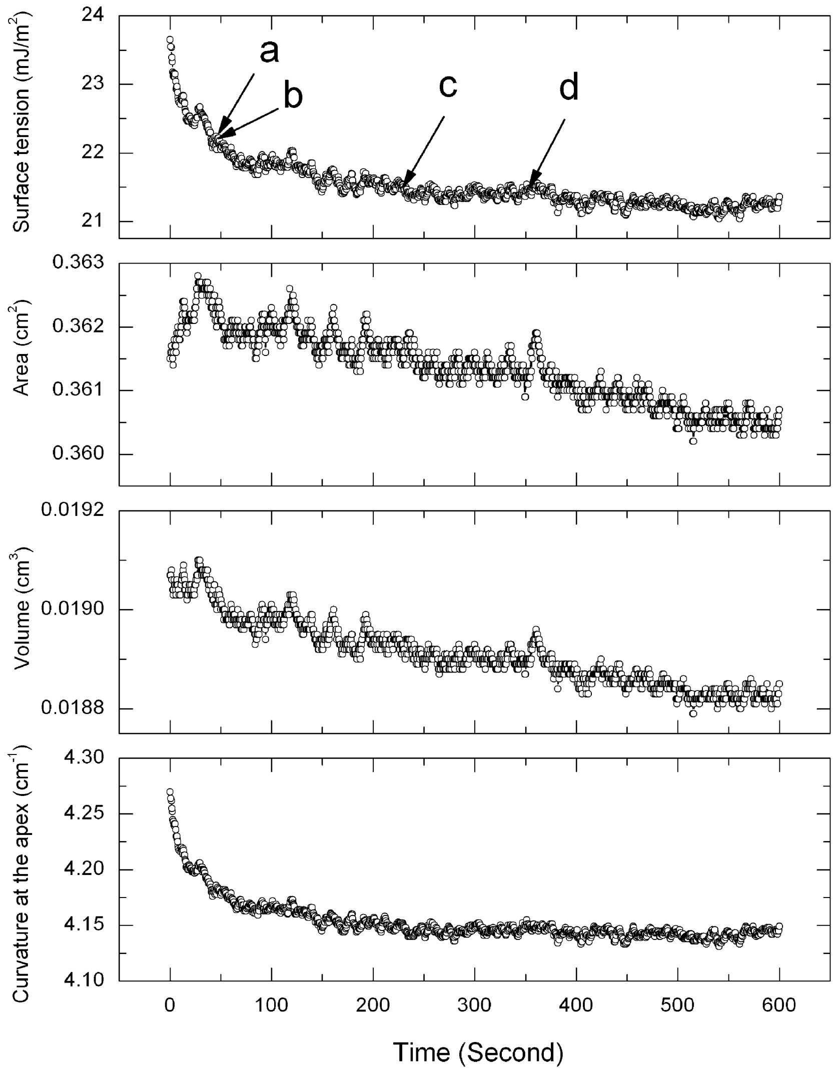

Fig. 3. ADSA results for a static experiment analyzed using the new version of ADSA-CB, for the same bubble as in Fig. 1; “a”, “b”, “c” and “d” denote the time points 40.07, 40.48, 226.95 and 350.54 s, respectively.

fluctuation of surface tension. To further elaborate on this point, Fig. 4 shows the fine structure of isotherms for surface tension, curvature at the bubble apex, and volume, which are enlarged from Fig. 3 in the range of 100 to 300 s. It can be seen that the surface tension and curvature at the apex, which are optimized independently in ADSA, are correlated. Thus, the fine structure of surface tension is not an artefact, but a consequence of adsorption kinetics. The pattern is consistent with the expectation that aggregates of the lung surfactant are transported from the bulk to the surface, giving rise to a non-smooth evolution of surface concentration of lung surfactant.

Bubble volume as well as surface area are conceptually dependent on the surface tension through the Laplace equation of capillarity. However, it should be noted that the bubble volume and surface area given in Fig. 3 are not independent optimization parameters, but were calculated inside ADSA, using surface tension and curvature at the apex as input information.

It should also be noted that the fluctuations in volume and surface area are much smaller than those in surface tension. Fluctuations in surface tension are of the order of 2%, whereas bubble volume and surface area fluctuations are almost an order of magnitude smaller.

3.2.2. Dynamic cycling experiments

Fig. 5 shows the surface tension-relative area (γ–A) isotherms calculated for the first 10 cycles using the new version of ADSA-CB. It is seen that, to reach a surface tension less then 5 mJ/m^2, the compression ratio for all 10 cycles, including the first one right after the adsorption, is less than 20%.

For an insoluble film under dynamic conditions, film compressibility is a commonly used parameter to reveal the interaction between the molecules forming the film. However, film compressibilities calculated in previous studies with different methodologies are inconsistent. Using the new version of ADSA-CB, film compressibility at a

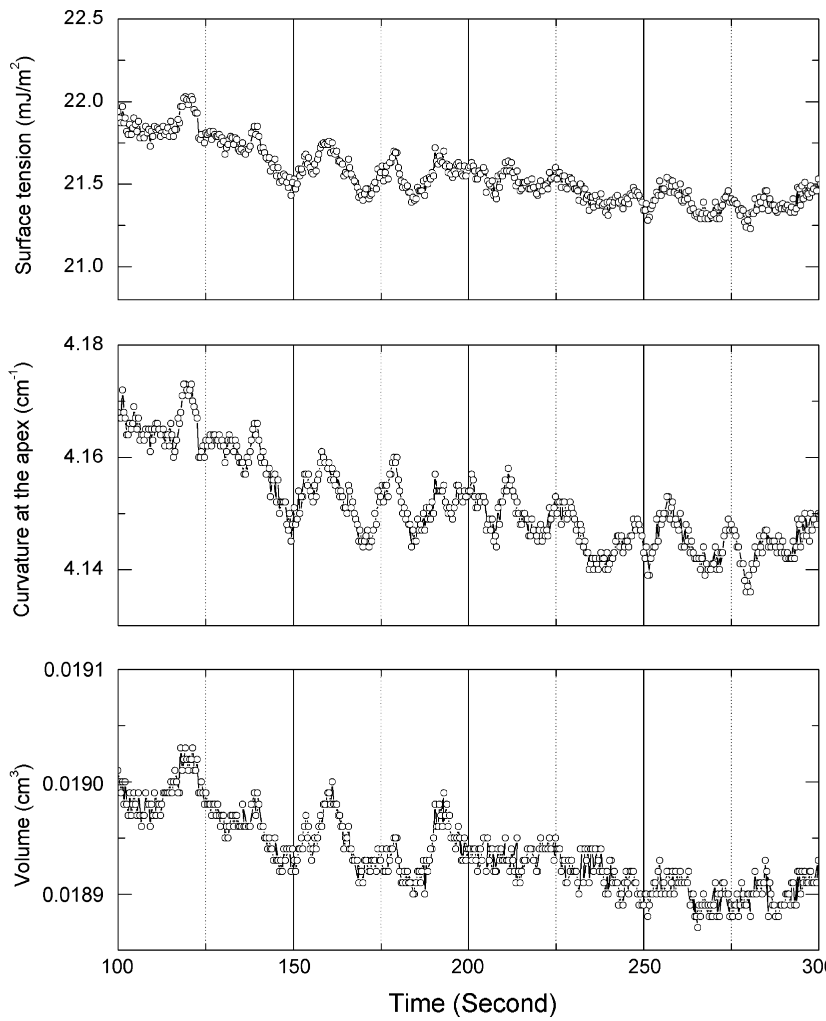

Fig. 4. Enlarged section of Fig. 3 for surface tension, curvature at the apex and volume.

surface tension of 15 mJ/m^2 calculated from the first compression is only 0.00700 (mN/m)$^{-1}$. The value for the subsequent 9 cycles is slightly smaller and constant at 0.00654$\pm$0.00006 (mN/m)$^{-1}$, indicating good reproducibility of this methodology. While these values may depend on the rate of compression, the intent here is to illustrate the difference between the first and the subsequent cycles. Presumably, the difference is due to squeeze-out of non-DPPC components from the film in the first cycle, as reported elsewhere [23–25].

4. Discussion

4.1. Shortcomings of thresholding

Thresholding has only limited suitability for processing a captive bubble image acquired in lung surfactant studies. This is due to the intrinsic noisy nature of bubble images. For a noisy image, it is very difficult to select an appropriate threshold value a priori since the histogram tends to lose the required bimodal shape [12]. ADSA results, especially the bubble area and volume, are found to be very sensitive to the threshold value. Errors caused by a poorly selected threshold value can produce significant inaccuracies. For instance, when gas transfer is studied from a sparingly soluble gas bubble, such as oxygen, to the surrounding quiescent aqueous solution, the total mass transfer rate over a relatively long period is of the same order of magnitude as these errors [26]. Therefore, for such a sophisticated study, thresholding as used in the first version of ADSA-CB [10] is not appropriate.

The noticeable dependence of ADSA results on the threshold value is due to the following. To find an edge, thresholding scans the working region in only two directions, the horizontal and vertical, regardless of the orientation of the edge. Thresholding may perform adequately for an edge perpendicular to the scanning direction. As the orientation of the bubble edge changes continuously along the profile, the transition region across the interface becomes elongated in the scanning direction. This causes difficulties in choosing a threshold value valid

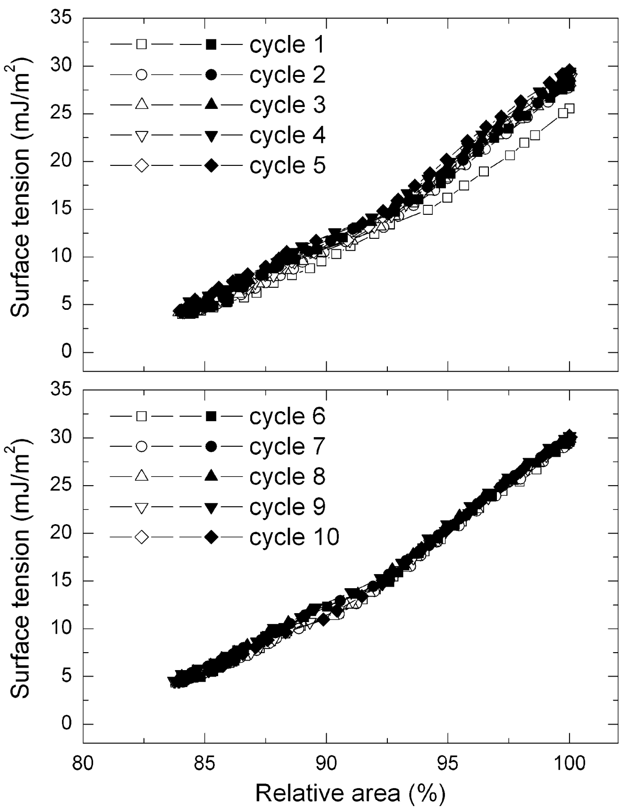

Fig. 5. Surface tension–relative area (γ–A) isotherms for the first 10 dynamic cycles after a rapid adsorption from a 0.5 mg/ml BLES suspension. Open symbols: compression; solid symbols: expansion.

for all parts of the edge. A relatively small threshold will force the edge scanning to go closer to or even enter the bubble regardless of the real position of the edge. Thus, the calculated bubble area and volume shrink with decreasing threshold value and swell when the threshold is moved in the opposite direction.

4.2. Noise resistance and self-adjustment of ADSA-CB

Dynamic surface/interfacial tension measurements for biological liquids are important in a variety of biomedical and physiological studies [27,28]. Captive bubble experiment in conjunction with a drop shape method was found to be a useful approach to conduct such dynamic surface/interfacial tension measurement [29,30]. However, the applicability of the captive bubble setup is significantly limited by the fact that most biofluids, such as lung surfactants, are turbid, even at relatively low concentrations.

The challenges of using ADSA-CB to study the dynamic processes of a biological liquid such as lung surfactant are (1) efficient noise reduction and (2) high degree of automation. The first requirement is needed to handle the noise of a captive bubble image as mentioned before; the second one is due to the fact that typically a large number of images need to be processed. It is impossible to deal with each image individually. Instead, the analysis should be conducted using one set of pre-determined input parameters without further human interference. Therefore, automation or self-adjustment is necessary.

The combination of the Canny edge detector and ALFI-S used in this new version of ADSA-CB is found to satisfy these two requirements. First, the Canny edge detector is robust against noise. Second, ALFI-S is very powerful in smoothing a Laplacian curve. ALFI-S is also self-adjusting, by means of an iteration algorithm and adaptive noise removal. The self-adjustment of ALFI-S can be seen from Fig. 6 where the new version of ADSA-CB is used to analyze the static experiment shown in Fig. 3. A satisfactory value of σ_G (i.e., 3.0) is selected according to the procedure described before [12]. Fig. 6 shows the number of iterations of ALFI-S, and the numbers of rejected and remaining edge points after performing ALFI-S. It is noticed that after AFLI-S, the number of remaining edge points remains approximately constant (720) for all the images in the same run. However, the numbers of rejected points and iterations keep varying automatically. For a less noisy image as shown in Fig. 2(a) (i.e., 40.07 s), the number of iterations is 5 and the number of rejected points is 24. In contrast, for an image with an adhering satellite bubble (as shown in Fig. 2(b), i.e.,

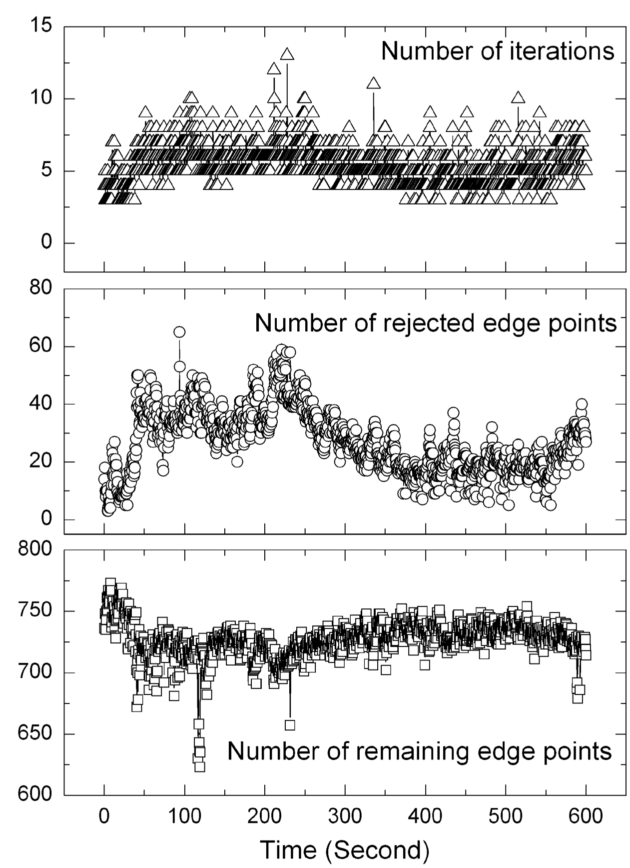

Fig. 6. Edge smoothing results outputted by ALFI-S for the static experiment shown in Fig. 3. The standard deviation of the Gaussian filter (σ_G) is selected as 3.0.

40.48 s), more iterations (7) are executed and more noise points (44) are deleted. For the extremely noisy image denoted by “c” in Figs. 1 and 3 (i.e., 226.95 s), 13 iterations are executed and 58 edge points representing the noise are deleted automatically.

It is also noted that, even though independent from each other, both the Canny edge detector and ALFI-S are indispensable to guarantee accurate and consistent ADSA results. The Canny edge detector provides high noise resistance, while ALFI-S can further reduce the noise without manual intervention. As a powerful free standing edge smoothing technique, ALFI-S can also be incorporated with the other edge detection or segmentation techniques. While ALFI-S would be expected to improve thresholding, it would not remove the fundamental problem connected with the choice of threshold, as discussed in Section 4.1. The reliable performance of the new ADSA-CB software should be attributed to both the Canny edge detector and ALFI-S.

Acknowledgements

This work was supported by a grant from Canadian Institute of Health Research (MOP-38037) and an Open Fellowship from University of Toronto to YYZ. We also thank Dr. David Bjarneson of BLES Biochemicals for his generous donation of the BLES samples.

References

[1] S. Schürch, H. Bachofen, J. Goerke, F. Possmayer, A captive bubble method reproduces the in situ behavior of lung surfactant monolayers, J. Appl. Physiol. 67 (1989) 2389–2396.

[2] S. Schürch, H. Bachofen, J. Goerke, F. Green, Surface properties of rat pulmonary surfactant studied with the captive bubble method: adsorption, hysteresis, stability, Biochim. Biophys. Acta 1103 (1992) 127–136.

[3] S. Schürch, H. Bachofen, F. Possmayer, Surface activity in situ, in vivo, and in the captive bubble surfactometer, Comp. Biochem. Physiol., A 129 (2001) 195–207.

[4] W.H. Schoel, S. Schürch, J. Goerke, The captive bubble method for the evaluation of pulmonary surfactant: surface tension, area, and volume calculation, Biochim. Biophys. Acta 1200 (1994) 281–290.

[5] J.D. Malcolm, C.D. Elliott, Interfacial tension from height and diameter of a single sessile drop or captive bubble, Can. J. Chem. Eng. 58 (1980) 151–153.

[6] Y. Rotenberg, L. Boruvka, A.W. Neumann, Determination of surface tension and contact angle from the shapes of axisymmetric fluid interfaces, J. Colloid Interface Sci. 93 (1983) 169–183.

[7] O.I. del Río, A.W. Neumann, Axisymmetric drop shape analysis: computational methods for the measurement of interfacial properties from the shape and dimensions of pendant and sessile drops, J. Colloid Interface Sci. 196 (1997) 136–147.

[8] S. Lahooti, O.I. del Río, P. Cheng, A.W. Neumann, Axisymmetric Drop Shape Analysis (ADSA), in: A.W. Neumann, J.K. Spelt (Eds.), Applied Surface Thermodynamics, in: M.J. Schick, F.M. Fowkes (Eds.), Surfactant Science Series, vol. 63, Marcel Dekker, New York, 1996, pp. 441–507, Chapter 10.

[9] R.M. Prokop, A.W. Neumann, Measurement of the interfacial properties of lung surfactant, Curr. Opin. Colloid Interface Sci. 1 (1996) 677–681.

[10] R.M. Prokop, A. Jyoti, M. Eslamian, A. Garg, M. Mihaila, O.I. del Río, S.S. Susnar, Z. Policova, A.W. Neumann, A study of captive bubbles with axisymmetric drop shape analysis, Colloids Surf., A Physicochem. Eng. Asp. 131 (1998) 231–247.

[11] J.Y. Lu, J. Distefano, K. Philips, P. Chen, A.W. Neumann, Effect of the compression ratio on properties of lung surfactant (bovine lipid extract surfactant) films, Respir. Physiol. 115 (1999) 55–71.

[12] Y.Y. Zuo, M. Ding, A. Bateni, M. Hoorfar, A.W. Neumann, Improvement of interfacial tension measurement using a captive bubble in conjunction with Axisymmetric Drop Shape Analysis (ADSA), Colloids Surfaces A: Physicochem. Eng. Aspects, in press.

[13] J. Canny, A computational approach to edge detection, IEEE Trans. Pattern Anal. Mach. Intell. 8 (1986) 679–698.

[14] E.N. Lightfoot, Transport Phenomena and Living Systems; Biomedical Aspects of Momentum and Mass Transport, Wiley, New York, 1974, pp. 387–393.

[15] T. Kuhl, Y. Guo, J.L. Alderfer, A.D. Berman, D. Leckband, J. Israelachvili, S.W. Hui, Direct measurement of polyethylene glycol induced depletion attraction between lipid bilayers, Langmuir 12 (1996) 3003–3014.

[16] D. Meyuhas, S. Nir, D. Lichtenberg, Aggregation of phospholipid vesicles by water-soluble polymers, Biophys. J. 71 (1996) 2602–2612.

[17] G. Putz, J. Goerke, J.A. Clements, Surface activity of rabbit pulmonary surfactant subfractions at different concentrations in a captive bubble, J. Appl. Physiol. 77 (1994) 597–605.

[18] P. Cheng, D. Li, L. Boruvka, Y. Rotenberg, A.W. Neumann, Automation of axisymmetric drop shape analysis for measurements of interfacial tensions and contact angles, Colloids Surf. 43 (1990) 151–167.

[19] P. Cheng, PhD thesis, University of Toronto, 1990.

[20] M. Hoorfar, A.W. Neumann, Axisymmetric Drop Shape Analysis (ADSA) for the determination of surface tension and contact angle, J. Adhesion, in press.

[21] G. Putz, J. Goerke, S. Schürch, J.A. Clements, Evaluation of pressure-driven captive bubble surfactometer, J. Appl. Physiol. 76 (1994) 1417–1424.

[22] P. Cheng, A.W. Neumann, Computational evaluation of axisymmetric drop shape analysis-profile (ADSA-P), Colloids Surf. 62 (1992) 297–305.

[23] J.N. Hildebran, J. Goerke, J.A. Clements, Pulmonary surface film stability and composition, J. Appl. Physiol. 47 (1979) 604–611.

[24] R.H. Notter, R. Taubold, R.D. Mavis, Hysteresis in saturated phospholipid films and its potential relevance for lung surfactant function in vivo, Exp. Lung Res. 3 (1982) 109–127.

[25] S. Schürch, D. Schürch, T. Curstedt, B. Robertson, Surface activity of lipid extract surfactant in relation to film area compression and collapse, J. Appl. Physiol. 77 (1994) 974–986.

[26] Y.Y. Zuo, PhD thesis, University of Toronto, in preparation.

[27] V.N. Kazakov, O.V. Sinyachenko, D.V. Trukhin, U. Pison, Dynamic interfacial tensiometry of biologic liquids—does it have an impact on medicine, Colloids Surf., A Physicochem. Eng. Asp. 143 (1998) 441–459.

[28] Elias I. Franses, O.A. Basaran, C.H. Chang, Techniques to measure dynamic surface tension, Curr. Opin. Colloid Interface Sci. 1 (1996) 296–303.

[29] R. Herold, H. Bünger, U. Pison, Assessment of pulmonary surfactant function using a captive-bubble surfactometer, Colloids Surf., A Physicochem. Eng. Asp. 114 (1996) 211–219.

[30] R. Wüstneck, N. Wüstneck, D. Vollhardt, R. Miller, U. Pison, The influence of spreading solvent traces in the atmosphere on surface tension measurements by using a micro-film balance and the captive bubble method, Mater. Sci. Eng., C 8–9 (1999) 57–64.